Nucleotide excision repair : complexes and complexities : a study of global genome repair in human cells

Volker, Marcel

Chapter 8

Xeroderma pigmentosum group A protein loads as a separate factor onto DNA lesions

adapted from
Mol. Cell. Biol. 23, no. 16, 5755–5767, August 2003

8 Xeroderma pigmentosum group A protein loads as a separate factor onto DNA lesions

Suzanne Rademakers,[1] Marcel Volker,[2] Deborah Hoogstraten,[1] Alex L. Nigg,[3] Martijn J. Moné,[4] Albert A. van Zeeland,[2] Jan H. J. Hoeijmakers,[1] Adriaan B. Houtsmuller,[3] and Wim Vermeulen

1 Center for Biomedical Genetics, Medical Genetic Center-Department of Cell Biology and Genetics, Erasmus Medical Center, P.O. Box 1738, 3000 DR Rotterdam
2 Medical Genetic Center-Department of Radiation Genetics and Chemical Mutagenesis, Leiden University Medical Center, Wassenaarseweg 72, 2333 AL Leiden
3 Josephine Nefkens Institute, Erasmus Medical Center, Department of Pathology, 3000 DR Rotterdam
4 Swammerdam Institute for Life Sciences, BioCentrum Amsterdam, University of Amsterdam, Plantage Muidergracht 12, 1018 TV Amsterdam

Abstract

Nucleotide excision repair (NER) is the main DNA repair pathway in mammals for removal of UV-induced lesions. NER involves the concerted action of more than 25 polypeptides in a coordinated fashion. The xeroderma pigmentosum group A protein (XPA) has been suggested to function as a central organizer and damage verifier in NER. How XPA reaches DNA lesions and how the protein is distributed in time and space in living cells are unknown. Here we studied XPA in vivo by using a cell line stably expressing physiological levels of functional XPA fused to green fluorescent protein and by applying quantitative fluorescence microscopy. The majority of XPA moves rapidly through the nucleoplasm with a diffusion rate different from those of other NER factors tested, arguing against a preassembled XPA-containing NER complex. DNA damage induced a transient, ~5-min immobilization of maximally 30% of XPA. Immobilization depends on XPC, indicating that XPA is not the initial lesion recognition protein in vivo. Moreover, loading of replication protein A on NER lesions was not dependent on XPA. Thus, XPA participates in NER by incorporation of free diffusing molecules in XPC-dependent NER-DNA complexes. This study supports a model for a rapid consecutive assembly of free NER factors, and a relatively slow simultaneous disassembly, after repair.

Introduction

DNA-damaging agents continuously challenge the integrity of DNA. DNA lesions directly affect transcription and replication, leading to cell death and contributing to aging, and also induce mutations that eventually cause carcinogenesis (13). Various repair mechanisms have evolved to prevent the consequences of DNA injuries and to preserve genetic integrity (21, 27). In mammals, the nucleotide excision repair (NER) process is the most important repair pathway for removal of UV light-induced lesions, including cyclobutane pyrimidine dimers, CPDs and 6-4 photoproducts and a wide range of helix-distorting chemical adducts. The significance of a functional NER system is apparent from the severe clinical features expressed by individuals suffering from the hereditary disorders xeroderma pigmentosum (XP), Cockayne syndrome (CS), and trichothiodystrophy (TTD) (7). Patients suffering from the prototype repair disorder XP are extremely sensitive to solar (UV) exposure, have an increased risk for skin cancer, and frequently exhibit neurological symptoms.

Detailed biochemical studies have shown that >25 polypeptides are required for in vitro NER (4, 15, 38). Two distinct NER subpathways operate within mammals, transcription-coupled repair (TCR) and global genome repair (GGR), each addressing a specific genome compartment and category of damages (10, 25). The distinction between these subpathways originates from the first steps of the mechanism, i.e., lesion detection. Lesions that block RNA polymerase II transcription elongation are preferentially repaired by TCR and require the CSA, CSB, and XAB2 proteins (45). TCR allows rapid resumption of the vital process of RNA synthesis and is particularly important for lesions that are inefficiently repaired by GGR-NER, such as CPDs. Injuries anywhere in the genome are targeted by the slower operating GGR. Damage sensing in this process is performed by the XPC/hHR23B/centrin 2 heterotrimeric complex (2, 52, 53, 60). In addition, the DNA damage binding, UV-DDB protein complex (9, 33) helps to identify CPDs in GGR (31, 35, 53, 56). On the other hand, a complex consisting of XPA and the single-stranded DNA binding protein RPA (replication protein A) (37) has been suggested to be the primary lesion detector in GGR (61), but this finding was recently challenged by Reardon and Sancar, who claimed that only RPA is the initial damage sensor (48).

The next step in NER is performed by the nine-subunit TFIIH complex (60, 64), containing the XPB and XPD helicases. TFIIH locally opens the DNA double helix around the lesion (20, 22), likely in the presence of XPG. Subsequently, XPA and RPA play an essential but as yet not fully understood role in the core of the reaction. XPA and RPA are necessary for further assembly and proper orientation of the incision proteins ERCC1/XPF and XPG (14). The latter are structure-specific endonucleases incising the damaged strand around the lesion (5′ and 3′, respectively), leaving an excised stretch of ~30 nucleotides. DNA polymerase δ/ε and auxiliary factors fill the remaining gap, which is sealed by ligase 1 (15, 27, 38).

Despite detailed knowledge of the in vitro NER mechanism, little is known about how this process operates in living cells. Different models for the organization of NER have been proposed, ranging from an ordered assembly of factors (1, 38, 44, 60) or four defined subcomplexes (23, 48, 61) to a preassembled NER holocomplex (54). Recently, our group provided evidence that some of the NER constituents roam through the nucleoplasm by diffusion and are transiently bound to complexes actively engaged in NER (28, 29). The XPA protein plays a crucial role within NER, since in the absence of this protein NER is completely abolished. Multiple interactions of XPA with other NER factors have been reported, suggesting a central role in complex assembly (14). These include the XPA/RPA complex exhibiting a higher specificity and affinity for damaged DNA than XPA alone and the ERCC1/XPF/XPA ternary complex, as well as an association with TFIIH (summarized in references 5 and 15). In addition, a link between XPA and TCR was suggested by the observed associations of CSB with the core NER factors XPA, XPG, and TFIIH (32, 51) and between XPA and XAB2 (45).

To provide further insight into the molecular interactions of XPA in living cells, we tagged this central NER factor with the green fluorescent protein (GFP) and studied its distribution and mobility in living cells. We applied fluorescence-based imaging and bleaching (fluorescence redistribution after photobleaching [FRAP]) methods using confocal laser scanning microscopy (29, 30) in cells containing local UV damage (43, 60). In similar previous studies of the NER factors ERCC1 and TFIIH (28, 29) our group provided evidence that at least these proteins do not reside in large NER holocomplexes. Here we present our findings on the dynamic properties of XPA-GFP, NER reaction kinetics, and the mode of complex assembly in living cells.

Materials and methods

Cell lines

Cell lines used in this study were the simian virus 40 (SV40)-immortalized fibroblasts MRC5 (wild type), XP2OS (XP-A), XP12RO (XP-A), and XP20MA (XP-C). These were cultured in RPMI$^+$-HEPES medium supplemented with antibiotics and 10% fetal calf serum at 37°C in an atmosphere of 5% CO_2. Primary fibroblasts used for microneedle injection, C5RO (wild type) and XP25RO (XP-A), and those used for immunofluorescence studies, VH25 (wild type), XP25RO (XP-A), XP21RO (XP-C), XPCS1RO (XP-G/CS), XP1DU (XP-D), XP8BR (XP-D/CS), and XP131MA (XP-B/CS), were cultured in Ham's F10 medium supplemented with antibiotics and 15% fetal calf serum.

Generation of GFP-tagged XPA

GFP-tagged XPA was generated by in-frame ligation of an XPA cDNA fragment (nucleotides 9 to 863) encoding the entire XPA, except for the first three amino acids, into pEGFP-C1 (Clontech). His_9 and hemagglutinin (HA) tags were both added to the N terminus of enhanced GFP (eGFP). The His_9-HA encoding sequence was introduced via ligation of a double-stranded oligonucleotide at the N terminus of eGFP after *Nhe*I-*Nco*I digestion (5′ CTAGCAAC ATG GGC CAC CAC CAT CAC CAT CAT CAC CAC CAC GGC **TAC CCA TAC GAT GTT CCA GAT TAC GCA AGC** GC 3′), resulting in a fusion gene under the control of a cytomegalovirus promoter encoding a 9-histidine stretch (underlined)-HA tag (bold)-eGFP–XPA hybrid polypeptide.

Microneedle injection and UDS

Microinjection of cDNA into cultured, multinucleated primary XP-A (XP25RO) fibroblasts was performed as described previously (59). After injection, cells were incubated for 24 h at 37°C in standard medium to allow expression of the cDNA. Fluorescent (GFP) images were obtained with an Olympus IX70 microscope (excitation at 455 to 490 nm band pass filter, long pass emission filter, >510 nm). DNA repair capacity was determined by measuring unscheduled DNA synthesis (UDS). Fibroblasts were UV-irradiated at 16 J/m^2 (254 nm), pulse-labeled for 2 h using [^{3}H]thymidine (20 μCi/ml), and fixed for in situ autoradiography. Autoradiographic grains above the nuclei of injected polykaryons were counted and compared with the amount of grains above the nuclei of wild-type primary fibroblasts (C5RO) treated in parallel.

Transfection of human fibroblasts

XPA-and XPC-deficient human SV40transformed fibroblasts were transfected with the His9-HA-eGFP–XPA fusion expression plasmid containing the NEO gene by using SuperFect (Qiagen). Cells were diluted 24 h after transfection, and medium containing 0.3 mg of G418, gentamicin/ml was added. Gentamicin-resistant XP-A cells were subsequently selected for UV resistance by irradiation three times, with a 1-day interval with 4 J of UV-C/m^2. Surviving clones were further selected for the presence and proper expression level of nuclear fluorescence by cell sorting using a FACS-Vantage cell sorter (Becton Dickinson). eGFP fluorescence was excited at 488 nm with a 20-mW Ar laser, and eGFP emission was detected using a 525-nm dichroic shortpass mirror and a 530/30-nm bandpass filter.

Immunoblot analysis and UV survival

Whole-cell extracts prepared by sonication were separated by sodium dodecyl sulfate–11% polyacrylamide gel electrophoresis and transferred to nitrocellulose membranes. Expression of the fusion gene was analyzed by hybridizing the membranes with a polyclonal anti-XPA antibody (Santa Cruz), followed by a secondary antibody (goat anti-rabbit conjugated with horseradish peroxidase [Biosource International]), and detected using enhanced chemiluminescence, Amersham.

For UV survival experiments, cells were plated and exposed to different UV doses 2 days after plating. Survival was determined 3 days after UV irradiation by incubation at 37°C with [^{3}H]thymidine pulse-labeling as described elsewhere (24).

Immunofluorescence
Cells were grown on glass coverslips and fixed with 2% paraformaldehyde at 37°C. Coverslips were washed three times for 5 min with phosphate-buffered saline (PBS) containing 0.1% Triton X-100 and subsequently washed with PBS^+ (PBS containing 0.15% glycine and 0.5% bovine serum albumin). Cells were incubated at room temperature with primary antibody for 1.5 h in a moist chamber. Subsequently, coverslips were washed three times with PBS–Triton X-100 and PBS^+, incubated for 1 h with secondary antibody at room temperature, and again washed three times in PBS–Triton X-100. Samples were embedded in Vectashield mounting medium (Vector) containing 0.1 mg of DAPI (4′-6′-diamidino-2-phenylindole)/ml. Primary antibodies used for immunolabeling were as follows: rabbit polyclonal anti-XPA antibodies (kindly provided by K. Tanaka, Osaka University, Osaka, Japan), rabbit polyclonal anti-XPC (57), mouse anti-CPD monoclonal antibodies (gift from O. Nikaido, Kanazawa University, Kanazawa, Japan), and mouse monoclonal anti-RPA70. Secondary antibodies were as follows: Alexa 594-conjugated goat anti-rabbit antiserum (Molecular Probes) and Cy2-and Cy3-conjugated goat anti-mouse antiserum (Jackson ImmunoResearch Laboratories). Fluorescent microscopy images were obtained with a Leitz Aristoplan microscope equipped with epifluorescence optics and a PLANAPO 63X, 1.40-numerical aperture oil immersion lens or with a Zeiss Axioplan 2 microscope equipped with epifluorescence optics. Quantification of fluorescence signal was determined using macrocontrolled digital image analysis software (KS-400; Zeiss).

Confocal microscopy
Digital images of GFP-expressing living cells were obtained using a Zeiss LSM 410 microscope equipped with a 60-mW Ar laser (488 nm) and a 40X, 1.3-numerical aperture oil immersion lens. Images of single nuclei were taken at a sample interval of 100 nm. For analysis of GFP-XPA expression levels, confocal planes were scanned at relatively low resolution (625-nm sample interval). A computer-controlled acousto-optic transmission filter was used to vary the intensity of the line of an Ar laser. GFP fluorescence was detected using a dichroic beamsplitter (488/543 nm) and an additional 515 to 540-nm bandpass emission filter.

UV irradiation
For total UV DNA damage induction, cultured cells were rinsed with PBS and UV-irradiated on coverslips with a Philips TUV lamp (254 nm) at a dose rate of ~0.8 $J/m^2/s$. To apply local UV damage on living fibroblasts, cells were UV-irradiated through an isopore polycarbonate filter (Millipore) containing 5 μm-diameter pores as described previously (43, 60). Subsequently, after filter removal, cells were either cultured or microscopically examined or fixed with paraformaldehyde and further processed for immunocytochemistry as described above.

FRAP and fluorescence loss in photobleaching (FLIP)
FRAP experiments were used to determine the effective diffusion coefficient (D_{eff}) of GFP-labeled XPA (under various experimental conditions) (29, 30). Briefly, a narrow strip spanning the entire nucleus was bleached for 200 ms at high laser intensity (100% of the 488-nm line of a 60-mW Ar laser). Subsequently, the recovery of fluorescence in the strip was monitored at intervals of 100 ms at 5% of the laser intensity applied for bleaching. The effective diffusion coefficient (D_{eff}) was estimated by calculating the relative fluorescence intensities given by the equation $FR_t = (I_t - I_0)/(I_\infty - I_0)$, where I_∞ is the fluorescence intensity measured after complete recovery, I_0 is the fluorescence intensity immediately after bleaching, and I_t is the fluorescence intensity measured at different time points (at 100-ms intervals). The resulting curves were fit to a theoretical diffusion model as described previously (18) (1-D diffusion). In this model, fluorescence recovery (FT) is defined by the equation $FT_t = 1 - [w^2 \times, w^2 + 4D\pi t^{-1}]^{½}$, where w is the width of the bleached strip, D is the diffusion coefficient, and t is time. The optimal fit was found by minimizing $\Sigma(FR_t - FT_t)^2$ (ordinary least squares) for both the diffusion coefficient (D) and the fluorescence intensity immediately after bleaching (I_0). The immobile fraction, FR was calculated from the equation $FR = 1 - [(I_\infty - I_0)/(I_{t<0} - I_0)] - (N_{mobile,bleached}/N_{tot})$, where N represents the number of molecules, $I_{t<0}$ and I_0 are the fluorescence intensities immediately before and after bleaching, respectively, and I_∞ is the fluorescence intensity measured after complete recovery. $N_{mobile,bleached}/N_{tot}$ is subtracted to correct for the fraction of mobile molecules in the relatively small volume of the nucleus that were bleached by the high-intensity laser pulse.

The immobilization measurements of GFP-labeled molecules were performed using a modified FRAP assay (FRAP-FIM [FRAP for immobilization measurements]) as described previously (29, 30). Using this method, quantitative fluorescence over a confocal plane of the entire nucleus was measured. Briefly, a small spot in the center of the nucleus was bleached at low laser intensity for a relatively long period (4 s at relatively low laser intensity [15% of a 60-mW Ar laser]) with the aim of bleaching a significant proportion of the GFP-tagged molecules in the nucleus. Subsequently, after an additional 4 s, a postbleach image was made and compared with a prebleach image of the same focal plane. The fluorescence intensity ratio (I_{post}/I_{bleach}) was plotted as a function of distance to the laser bleach spot, generating a fluorescence ratio profile (FRP) (see Fig. 4). Chemically immobilized molecules, paraformaldehyde fixation were used as 100% immobilization controls.

FLIP experiments were used to determine the residence time of GFP-tagged XPA molecules in local UV-irradiated areas (see above). For this, a strip at a relatively long distance from the site of local damage was photobleached for 4 s at relatively low laser intensity. Subsequently, fluorescence intensity was monitored in the local damage area, in the bleached area, and in an undamaged control region located at the same distance from the bleached area as the local damage area. The difference between the fluorescence in the damage area and that in the control region was plotted and the time at which 10% of the initial difference was reached was taken as an estimate for the residence time of individual molecules associated with the local damage area.

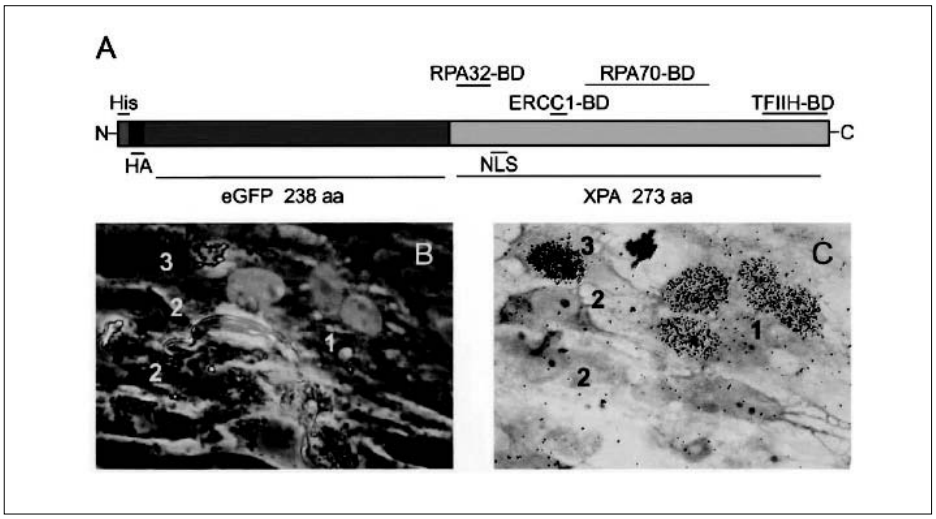

Figure 1. Functionality of GFP-XPA
(A) Schematic representation of the His9-HA-eGFP–XPA fusion gene with the different binding domains indicated. NLS, nuclear localization signal; BD, binding domain; aa, amino acids. (B) Fluorescence image of XP-A cells injected with GFP-tagged XPA cDNA. Only the multinucleated cell microinjected with GFP-XPA cDNA showed a homogeneous nuclear expression (number 1); surrounding cells were not injected (number 2). (C) Measurement of the repair capacity of cells with fluorescent nuclei by means of UV-induced UDS (see Materials and Methods). The amount of silver grains above the nuclei of the injected cells (number 1) was comparable to what was seen with wild-type cells (not shown), whereas the surrounding XP-A fibroblasts (number 2) show the low level of DNA synthesis typical for UV-exposed XP-A cells. The cell indicated with the number 3 is in S phase. See the Appendix for a colour version of this figure.

Results

Construction and characterization of GFP-XPA

The XPA cDNA was fused to the eGFP cDNA containing histidine and HA tags at its N terminus, see Materials and Methods, resulting in a His_9-HA-eGFP–XPA hybrid gene (designated GFP-XPA) (Fig. 1A). To verify that the GFP tag did not interfere with the XPA function, the fusion gene was microinjected into nuclei of XPA-deficient human fibroblasts. One day after

microinjection a bright fluorescent signal within the nuclei of injected cells was observed (Fig. 1B). Fluorescent cells were recorded and assayed for their repair capacity by determining UV-induced UDS. As shown in Fig. 1C, the cells with green fluorescent nuclei (Fig. 1B) were also corrected (up to wild-type levels) for the severe UDS defect present in XP-A cells (noninjected neighboring cells). Both nuclear targeting and the complete restoration of UDS indicate that the His9-HA-eGFP tag does not interfere with the proper function of XPA when transiently expressed in XP-A cells.

Generation and characterization of cells expressing GFP-XPA

To investigate the in vivo distribution of GFP-XPA in time and space, the fusion gene was stably expressed in an XPA-deficient human SV40-immortalized fibroblast. We isolated several UV-resistant clones and analyzed the expression levels of the fusion proteins by immunoblotting (data not shown). We selected a clone (clone 40) that expressed the fusion protein to near normal levels compared with XPA expression in wild-type cells (Fig. 2). As observed previously, wild-type XPA migrates as two distinct bands in polyacrylamide gel electrophoresis (40 and 42 kDa) (17, 42, 49); the fusion protein is also present in two forms, migrating at the expected positions of ~68 and ~70 kDa. Immunostaining with anti-GFP (data not shown) revealed that there was no detectable free GFP present in the crude extracts. UV survival experiments demonstrated that tagged XPA restores the extreme UV-sensitive phenotype of XP-A cells to the wild-type range (Fig. 2B). This confirms the UDS results of the microinjection at physiological protein levels in stably expressing transformants.

GFP-XPA appeared to be homogeneously distributed in living nuclei (Fig. 2C and D), including the nucleoli. In approximately 40% of the cells, a few (1 to 5) bright fluorescent spots were observed. GFP signal in fixed cells (Fig. 2E) and immunofluorescence, anti-XPA (Fig. 2F) displayed a similar distribution as in living cells (Fig. 2D), except that nucleoli seemed devoid of XPA after immunofluorescence (Fig. 2F), similar to what has been reported previously (42). The lack of nucleolar staining by immunofluorescence might be caused by the fixation procedure which renders this highly condensed organelle less permeable for antibodies (63). Although UV-C irradiation slightly reduced the number of cells containing spots, the overall distribution pattern did not change (data not shown). At present, the nature and significance of these foci remain unknown. Similar structures have been found in ERCC1-GFP-expressing cells (29).

Diffusion of GFP-tagged XPA

Prior to mobility studies of GFP-XPA in living cells, we first analyzed the expression level of individual cells in clone 40. Immunofluorescence with anti-XPA serum was performed on a (1:1) mixed population of wild-type (MRC5) and clone 40 cells. The frequency distribution (Fig. 2G) shows that both the level of expression and the intercellular variation are comparable, with the exception of a small fraction of cells overexpressing GFP-XPA. Only cells (from clone 40) with a modal expression level equivalent to that of wild-type cells were used in further quantitative fluorescent experiments, unless stated otherwise.

Mobility measurements to determine whether GFP-XPA molecules are mobile or bound to nuclear structures were performed by applying FRAP. Here we used the strip-FRAP method (see Materials and Methods and reference 30 for detailed information) to measure the mobility. Briefly, GFP-XPA molecules were photobleached in a defined narrow strip spanning the nucleus (strip-FRAP). The speed of recovery is a measure for the diffusion rate of the molecules, and the degree of fluorescence recovery indicates whether (part of) the GFP-XPA molecules are mobile.

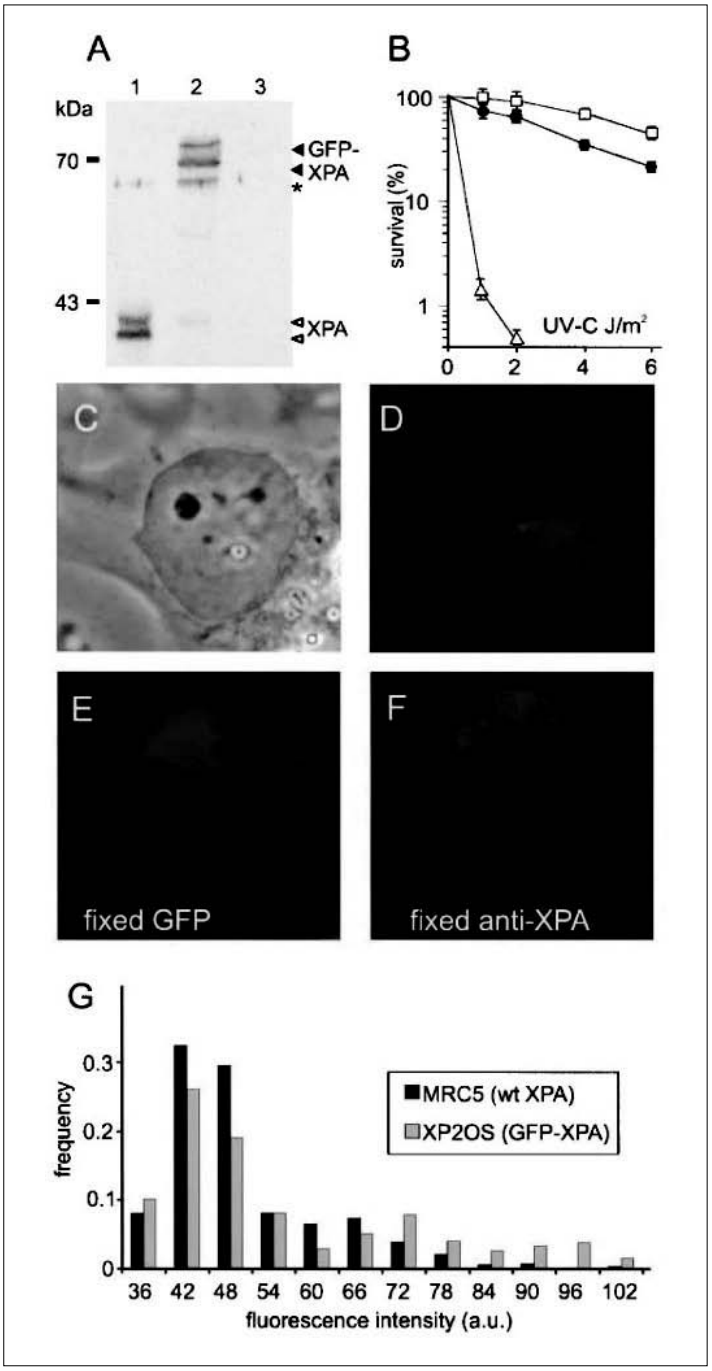

Figure 2. Expression and characterization of XP2OS cells stably expressing GFP-tagged XPA
(A) Immunoblot of 30 µg of whole-cell extract from MRC5, wild-type (lane 1), GFP-XPA-transfected XP2OS (clone 40) (lane 2), and XP2OS, XP-A (lane 3) cells probed with polyclonal anti-XPA. The molecular masses of protein markers are indicated in kilodaltons. No XPA protein was detected in XP2OS cells because of a G-C transversion in the splicing acceptor site in intron 3 of the XPA gene. The asterisk indicates a nonspecific crossreacting band. (B) UV survival of repair-proficient MRC5 cells (□), clone 40 (■) and XP2OS cells (△) (see Materials and Methods). The transfected cell line shows a wild-type correction of the XP-A-specific UV sensitivity. (C) Phase-contrast image of a living clone 40 cell. (D) Epifluorescence GFP image of the same cell as in panel C, showing a homogeneous nuclear distribution. (E) Fluorescence image after fixation of clone 40, showing a similar distribution as in panel D. (F) Immunofluorescence of the same cell as in panel E incubated with anti-XPA serum, showing a similar XPA distribution as with GFP fluorescence, except for the nucleoli. (G) Expression profiles of XPA (black bars) and GFP-XPA (gray bars) in MRC5 cells and clone 40, respectively, after immunofluorescence staining with XPA antibodies. GFP-XPA cells exhibiting an expression level similar to the major peak of XPA expression in MRC5 cells were used in further experiments. See the Appendix for a colour version of this figure.

For chemically fixed cells, no recovery was observed, as expected (Fig. 3A and B). In contrast, in living cells the vast majority of GFP-XPA appeared to be mobile (Fig. 3C and D). The kinetics of recovery yielded an effective diffusion coefficient (D_{eff}) for GFP-XPA of 15 ~2 µm²/s. This D_{eff} is much higher than that of XPB-GFP (6 ~1 µm²/s), part of TFIIH, and we found it in repeated experiments to be higher than that of ERCC1-GFP/XPF (12 ~2 µm²/s) assayed in parallel. These data suggest that in undamaged cells the majority, >95% of XPA is not incorporated into a stable large complex and diffuses freely as single molecules (or part of small transient subcomplexes) throughout the nucleoplasm.

DNA repair-dependent immobilization of GFP-XPA

To investigate the effect of the presence of DNA damage on XPA mobility, we performed FRAP analysis on cells exposed to UV-C (16 J/m^2, an NER-saturating dose) (Fig. 3E and F). The reduced fluorescence recovery, visible 2 s after bleaching (Fig. 3F [compare with nontreated cells shown in Fig. 3D]), and the lower recovery of the diffusion plot (Fig. 3G) are indicative for an immobilized fraction. The relative amount of binding (maximally ~35%) depends on the expression level, since cells expressing high levels of GFP-XPA show a proportionally smaller immobilized fraction compared with cells expressing moderate amounts of GFP-XPA (Fig. 3G). This suggests that at a given UV dose the total number of molecules participating in the DNA repair reaction (i.e., immobilization) is roughly the same in all cells independent of the expression level. The D_{eff} of the free fraction of GFP-XPA molecules did not change after damage induction (13 ~2 μm^2/s) (Fig. 3G), indicating that the free molecules were not incorporated into larger (mobile) complexes.

To more precisely quantify the DNA damage-induced immobilization of GFP-XPA, we used a different FRAP procedure, FRAP-FIM, as described previously (29, 30). FRAP-FIM measurements (the mean results for at least 30 cells and typical examples of cells) are shown in Fig. 4. In accordance with the strip-FRAP analysis, these measurements showed a UV light-dependent (and maximally ~35%) immobilization of GFP-XPA (Fig. 4G to J). These results indicate that the number of immobilized molecules depends on the number of lesions. In addition, the total amount of immobilized molecules, as shown above, does not depend on the amount of available GFP-XPA molecules, suggesting that XPA is not the rate-determining factor of NER in the cell line investigated. Note that these experiments have been performed using SV40-im-mortalized cells that have reduced levels of tp53, which causes a decrease in GGR capacity (8).

The fraction of bound GFP-XPA molecules (~35%) remained more or less unaltered over a period of a few (2 to 4) hours post-UV exposure. Subsequently, a gradual decrease of immobilized molecules was observed, with no significant binding 24 h after UV exposure (data not shown). Previous studies ported for ERCC1-GFP (29), and not observed in cells ex-have shown that 24 h after UV exposure most UV-induced pressing single GFP or GFP-tagged RAD52 group proteins lesions have been removed by NER, suggesting full release of (19). In summary, the above findings are consistent with the bound molecules when repair is completed. This UV-induced idea that after DNA damage GFP-XPA molecules become immobilization is specific for NER proteins, as previously re-transiently immobilized by engagement in NER.

Local damage in GFP-XPA cells

To monitor the translocation of GFP-XPA molecules to damaged DNA in living cells and to determine the transient binding (or residence) time within NER complexes, we applied a novel technique for introducing UV damage to a restricted area of the nucleus (43, 60). Cells were covered with a polycarbonate filter that shields UV light and contains (5 μm-diameter) pores (Fig. 5A), causing DNA damage after UV exposure only at the positions of the pores. Shortly after UV irradiation (<5 min, i.e., the first time point analyzed), a clear accumulation of GFP-XPA molecules in restricted parts of the nuclei of living cells was observed (Fig. 5C, arrows). These GFP-XPA accumulations colocalize with XPC (Fig. 5D and E) and with CPDs (see Fig. 7D and E) and confirm that XPA preferentially localizes to sites of DNA damage (60). These observations suggest a model in which, free diffusing GFP-XPA molecules bind rapidly to damaged DNA-NER complexes in which they were transiently entrapped. To determine the residence time of GFP-XPA within these locally damaged areas, we applied FLIP (see Materials and Methods). At a position opposite to the damaged domain, a single pulse was used to bleach a small region

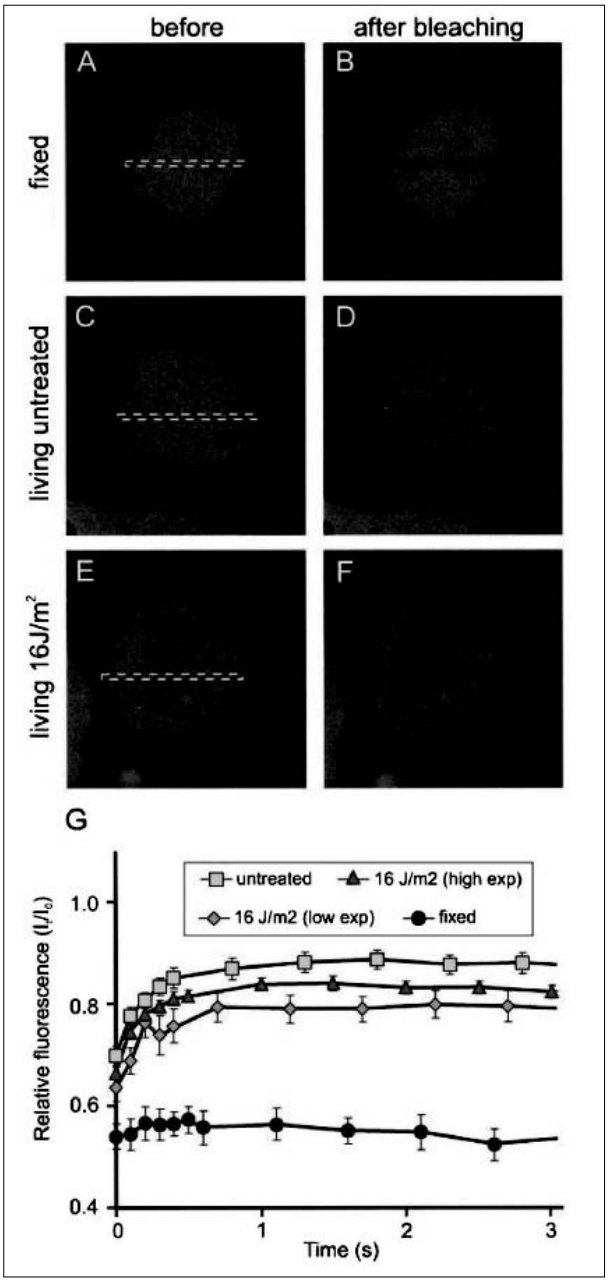

Figure 3. Temporal FRAP analysis applied on GFP-XPA-expressing cells to determine the immobile fraction after UV irradiation

Shown are confocal images and corresponding FRAP profiles. The dotted line indicates the position of the photobleaching strip. To determine a potential immobile fraction, the mean intensity immediately before bleaching was set as 1 and the fluorescence intensity immediately after bleaching was set as 0. (A and B) Pre- and postbleach images, respectively, of fixed cells, showing complete immobilization of GFP-XPA. (C and D) Images of living cells monitored during FRAP, with panel D showing a homogeneous bleaching throughout the nucleus 4 s after the bleach pulse. (E and F) Images of living cells irradiated with 8-J/m^2 UV-C. Note that the UV-irradiated cell (F) shows an intermediate pattern between those of untreated (D) and fixed (B) cells. (G) Fluorescence recovery profile expressed as relative fluorescence plotted against time after bleaching. Each plot is the mean value for at least 50 cells, fixed cells, untreated living cells, UV-irradiated cells expressing relatively low levels of GFP-XPA, and UV-irradiated cells expressing high levels of GFP-XPA. The immobile fraction can be calculated by measuring the reduction of fluorescence recovery compared with nonirradiated cells.

in the nucleus (Fig. 6B, inset). Both bleached and nonbleached molecules will distribute and mix, resulting in an overall decrease in fluorescence intensity. The time required to establish the initial (prebleach) fluorescence difference between the damaged area and the nucleoplasm is a measure for the mean residence time of molecules in that area. A typical series of images of this FLIP measurement is shown in Fig. 6A. The residence time for GFP-XPA was determined to be approximately 4 to 6 min (Fig. 6B). This residence time indicates the average binding period, or time of participation of GFP-XPA molecules within a single NER event.

GFP-XPA mobility in an XPC-deficient background

To obtain further evidence that immobilization is caused by actual engagement in NER, we studied the dynamic properties of GFP-XPA in a mutant NER background, i.e., an XPC-deficient (XP20MA-SV) cell line. Using fluorescence-activated cell sorting and immunoblot analyses (data

not shown), a clone was selected that expresses a relatively low level of GFP-XPA, approximately a 1:1 ratio with endogenous nontagged XPA.

FRAP-FIM measurements revealed that even after a high UV dose of 16 J/m^2 no significant immobilization of GFP-XPA was observed in XP-C cells (Fig. 7A and B). To study the absence of immobilization in an XPC-deficient background in more detail, local damage was applied to GFP-XPA-expressing, XPA- and XPC-deficient cells. GFP-XPA accumulates at locally damaged areas (using CPD antibodies) (Fig. 7C to E) only in the presence of XPC (Fig. 7, compare panels C to E with panels F to H [absence of XPC]). These observations clearly show that binding and transient immobilization of XPA molecules to damaged regions depend on the presence of functional XPC. Since XPC is only involved in GGR, these results further suggest that with the applied FRAP methods (and GFP-XPA), predominantly GGR is monitored, at least in the analyzed time periods after UV exposure.

Loading of XPA and RPA in the NER preincision complex

Our experiments indicated that incorporation of XPA into the NER preincision complex depends on the presence of XPC and that the XPA molecules get access to these lesions as a free diffusing entity. These dynamic studies do not, however, allow the determination of whether (part of the XPA) molecules are complexed to other (small) nuclear factors, such as RPA. It has been suggested that XPA is bound to the heterotrimeric RPA (26, 37, 39). Moreover, it has

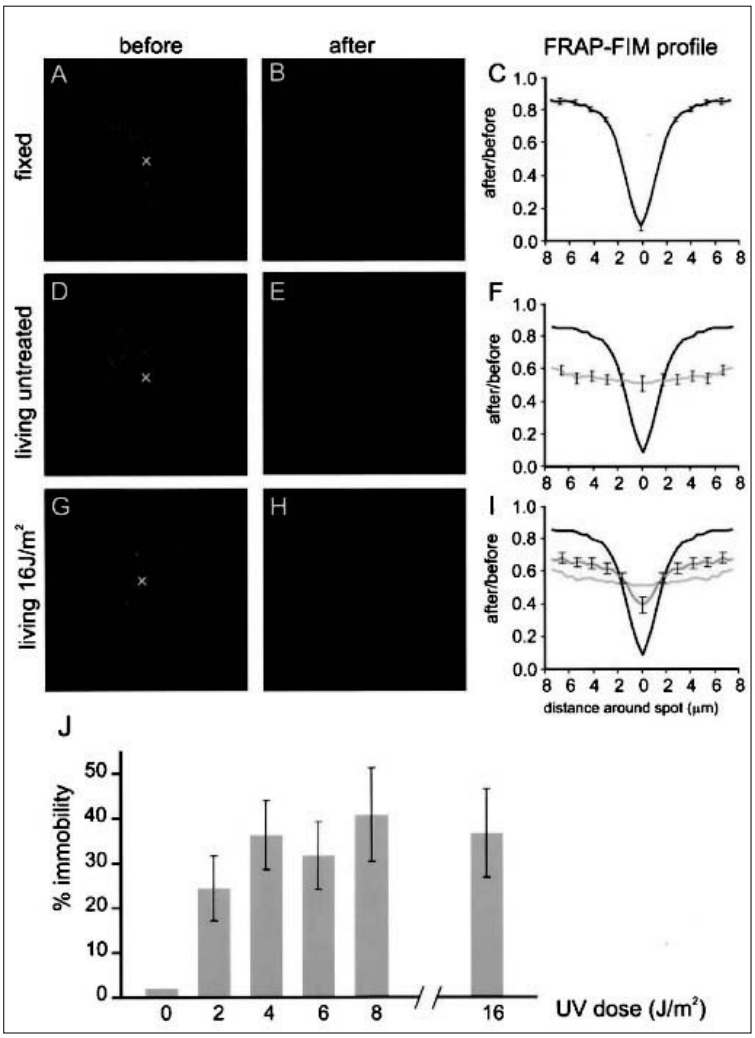

Figure 4. FRAP-FIM method applied to GFP-XPA-expressing cells
Shown are confocal images and corresponding fluorescence ratio profiles (FRP) of 50 cells. (A and B) Pre- and postbleach images, respectively, of cells fixed with 2% paraformaldehyde, displaying the immobilization of GFP-XPA molecules after fixation, visualized by the intense bleached spot and high fluorescence intensity outside the bleached spot, (B). (C) FRP of fixed cells. (D and E) Images of living untreated cells, showing an overall reduction of fluorescence after the bleach pulse (E). (F) FRP of untreated cells (green line). (G and H) Image of cells irradiated with 8-J/m^2 UV-C. The UV-irradiated cell (H) displays a distribution pattern intermediate of those of untreated (B) and fixed (E) cells. The 'X' in panels A, D, and G represents the position of the bleach pulse. (I) FRP of UV-irradiated cells (blue line). (J) Response of GFP-XPA immobilization to different UV doses.

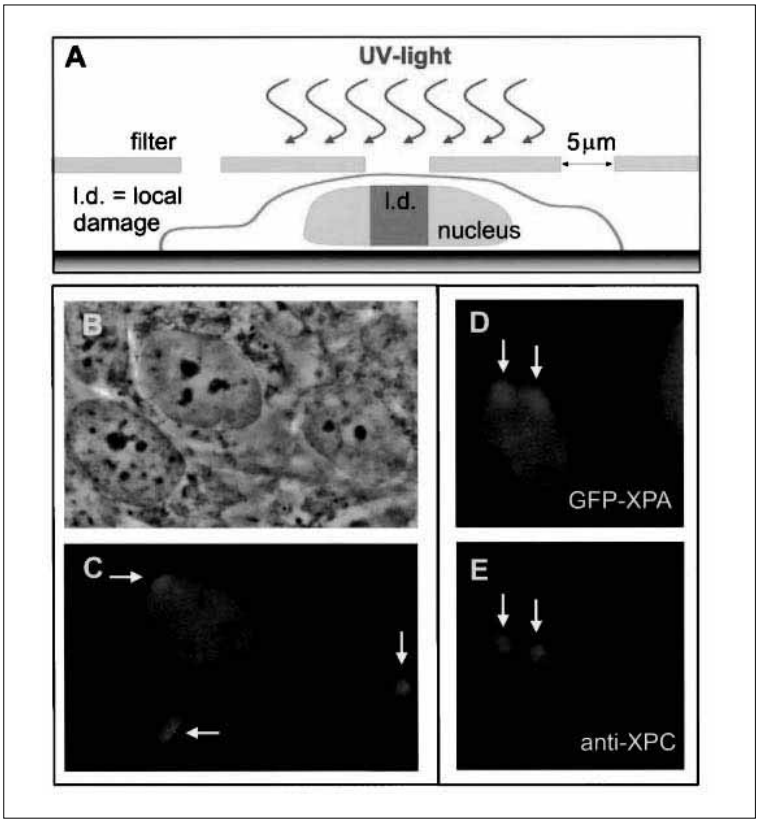

Figure 5. Accumulation of GFP-XPA within restricted nuclear areas after local UV irradiation
(A) Schematic presentation of local UV damage infliction on living cultured cells. (B and C) Micrographs, phase-contrast image [B] and fluorescence image [C] of living cells expressing GFP-XPA (clone 40) and UV-irradiated through a filter with small (5 µm-diameter) pores. The arrows in panel C point to the local accumulations of GFP-XPA. (D and E) GFP-XPA accumulations (arrows) shown in panel D clearly colocalize with endogenous XPC (E) concentrations, as determined with anti-XPC antibodies, in fixed cells. See the Appendix for a colour version of this figure.

been claimed that these proteins bind as a complex to DNA damage (61, 62). This XPA-RPA complex has a higher and more lesion-discriminative binding capacity than each of the separate proteins (41). To further investigate whether XPA gets access to the preincision complex as a single protein or in conjunction with RPA, we investigated the loading of RPA on UV lesions in a number of different NER factor-deficient cells.

In agreement with previous findings for other NER proteins (60), we found an accumulation of RPA in normal cells shortly after the introduction of local UV damage in the cell (Fig. 8A to C). The recruitment of XPA to the NER complex is not impaired in XP-G/CS cells (60), despite the virtual absence of XPG protein. Here we show that the relocalization of RPA to locally induced UV damage is also not impaired in these cells (Fig. 8D to F). This observation suggests that the recruitment of XPA and RPA is independent of XPG or alternatively that the XP-G/CS cells investigated might still express small amounts of truncated XPG protein that are sufficient to support recruiting of XPA and RPA.

Surprisingly, however, when we tested cells lacking XPA we also observed relocalization of RPA to the UV-damaged area of the nucleus with an efficiency similar to that in wild-type cells (Fig. 8G to I). This suggests that RPA is recruited to the NER complex on the basis of its affinity for single-stranded DNA, which is formed after the helix-unwinding action of TFIIH, or that other (protein-protein) interactions than those with XPA are sufficient to recruit RPA to the NER complex. Support for the latter explanation comes from our observations with XP-B/CS cells, which have been reported to lack helix opening in NER (20). In these cells, we could still observe RPA accumulation in sites of local UV damage (Fig. 8J to L). The same result was obtained with an XP-D/CS cell line bearing a mutation in the other helicase subunit, XPD of TFIIH (data not shown).

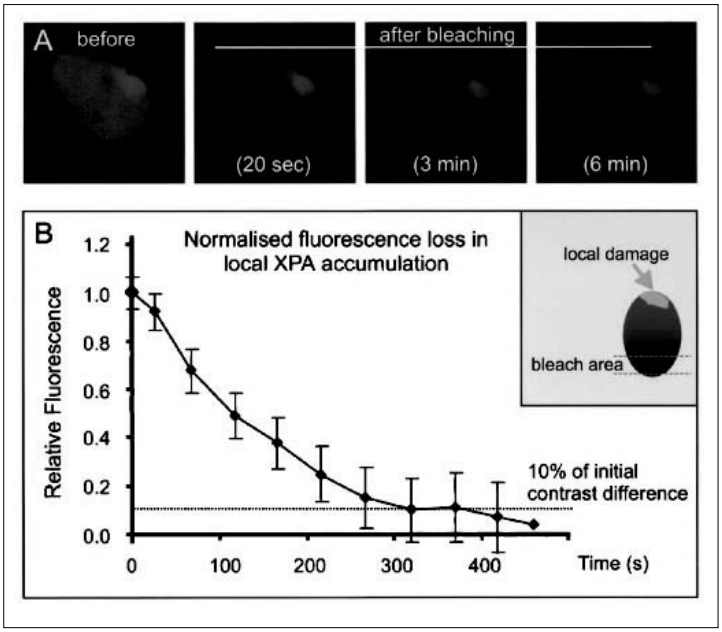

Figure 6. Application of FLIP, using locally damaged cells, to determine the binding time of GFP-XPA molecules on damaged DNA
(A) Confocal images of a locally UV-damaged GFP-XPA-expressing cell (clone 40). Shown are images before application of a bleach pulse and at 20 s, 3 min, and 6 min after bleaching. (B) Fluorescence profile as a function of time; residence time was estimated to be ~4 to 6 min, the time at which the relative fluorescence difference between damaged area and background is established to be <10% of the initial (prebleach) situation. The inset shows the application of the FLIP procedure in local damaged cells: a laser beam is focused (between dotted lines opposite to the damaged area (arrow) (a typical example is shown in panel A).

These findings are in accordance with recent observations by Patrick and Turchi (47), who presented evidence that initial binding of RPA to the damaged DNA is subsequently further stabilized by an interaction with XPA. Whether XPA is incorporated in the NER complex in vivo in the absence of RPA remains to be determined.

Furthermore, it has been suggested by Wakasugi and coworkers that the DDB protein complex might be responsible for the direct recruitment of XPA and RPA to sites of damage, without the need for the XPC/hHR23B complex (62). However, when we investigated XPC-deficient cells (that contain normal functional DDB complex) we found no accumulation of RPA in sites of local UV damage (Fig. 8M and N), in accordance with our previous findings that no NER proteins, including XPA, were found at sites of locally induced UV damage in XP-C cells. This observation together with our group's present and previous observations (60) support the notion that the visible assembly of the NER complex on a DNA lesion strictly depends on functional XPC protein, and we have found no evidence for direct recruitment of XPA and/or RPA by the DDB protein. Importantly, our observations are in contrast with the new order of assembly recently suggested by Reardon and Sancar (48), who describe a model in which RPA loading precedes XPC.

Discussion

The XPA protein plays an essential role in mammalian NER that until now has largely been assessed using biochemical and genetic means. In this study, we applied different variants of FRAP (30) on living cells stably expressing (at a biologically relevant level) functional GFP-XPA. These analyses provide insight into the hitherto unexplored in vivo spatiotemporal organization of this central NER factor.

The following observations indicate that the GFP-XPA-expressing cells accurately reflect the in vivo involvement of XPA in NER. (i) Expression in XPA-deficient cells established that the GFP-XPA protein is fully functional in NER in terms of UV survival and repair synthesis, despite the presence of the GFP tag, almost doubling the size of the protein. (ii) GFP-XPA is expressed at physiological levels, which is critical when analyzing the biologically active fraction of the

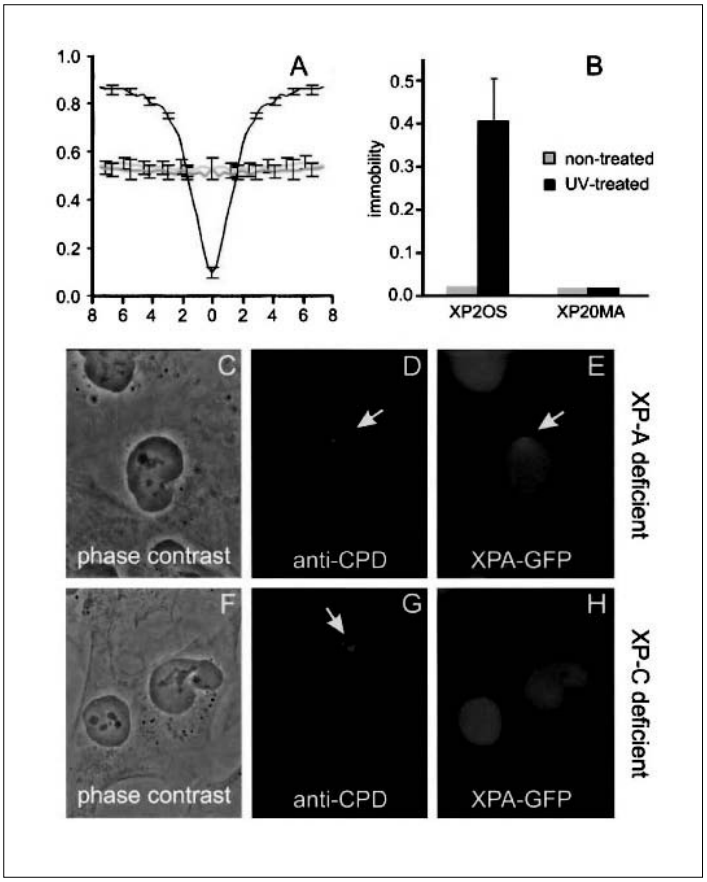

Figure 7. Effect of XPC on damage-induced XPA immobility as analyzed by FRAP-FIM and local damage induction
(A) FRAP-FIM profile of GFP-XPA expression in XP20MA (XP-C) cells. Shown are results for nonirradiated cells (light green line), cells irradiated at 16 J/m^2 (blue line), and fixed cells (black line). UV-exposed XP20MA cells do not show any GFP-XPA immobilization. (B) Quantification of immobilization of GFP-XPA in XP20MA and XP2OS cells with and without UV irradiation. (C) Phase-contrast image of GFP-XPA-expressing XP2OS cells. (D) Anti-CPD immunostaining in a GFP-XPA-expressing XP2OS cell. The arrow indicates the site of the damage. (E) GFP image of the same cell as in panel D, showing enrichment of GFP-XPA at the damaged site. (F) Phase-contrast image of GFP-XPA-expressing XP20MA cells. (G) Anti-CPD immunostaining of a GFP-XPA-expressing XP20MA cell, indicated by the arrow. (H) GFP image showing no enrichment of GFP-XPA molecules. See the Appendix for a colour version of this figure.

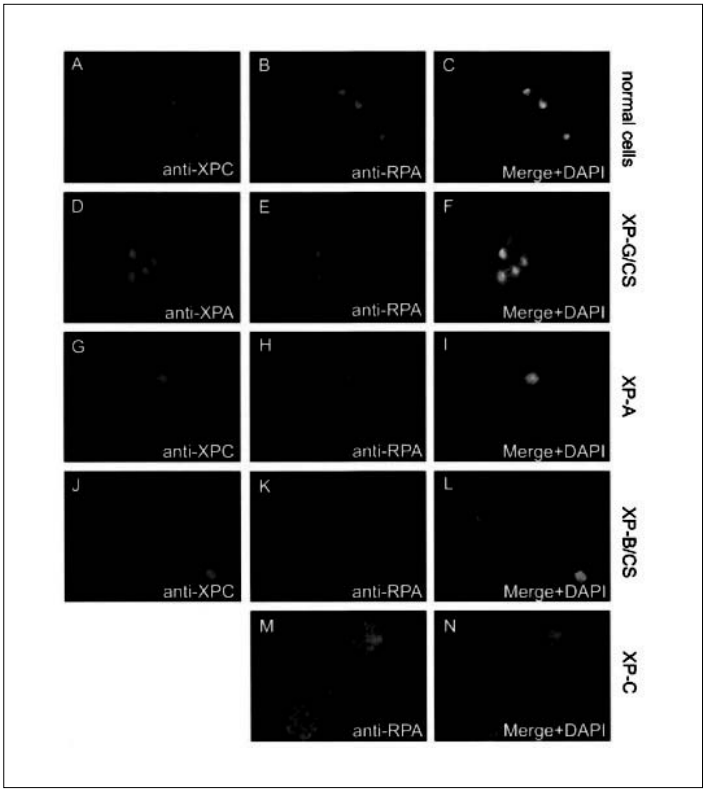

Figure 8. Relocalization of RPA to the NER complex 30 min after local irradiation with 25 J/m^2 UV
(A to C) Anti-XPC (A) and anti-RPA (B) immunostaining of VH25 cells and the merged image after immunostainings plus DAPI nuclear DNA staining (C). (D to F) Anti-XPA (D) and anti-RPA (E) immunostaining of XPCS1RO cells and the merged image after immunostainings plus DAPI nuclear DNA staining (F). (G to I) Anti-XPC (G) and anti-RPA, H immunostaining of XP25RO cells and the merged image after immunostainings plus DAPI nuclear DNA staining. (J to L) Anti-XPC (J) and anti-RPA (K) staining of XP131MA cells and the merged image after immunostainings plus DAPI nuclear DNA staining (L). (M and N) Anti-RPA immunostaining of XP21RO cells (M) and the merged image after immunostaining plus DAPI nuclear DNA staining (N). The yellow color in the merged images in panels C, F, I, and L indicates colocalization of NER proteins at sites of locally induced DNA damages. See the Appendix for a colour version of this figure.

protein. (iii) The subnuclear distribution is similar to that of wild-type, endogenous XPA (Fig. 1 and 2). (iv) As discussed below, the protein shows a consistent, direct, and specific response to NER-type DNA injury. Therefore, we consider this cell line to be a bona fide tool for studying the characteristics of XPA in living cells.

Organization of NER in living cells

Diffusion measurements in living cells indicated that the majority of GFP-XPA molecules are not part of a large, stable, preassembled NER complex. Obviously, we cannot exclude the possibility that a small fraction of XPA is incorporated into a larger functional NER (holo)complex. However, it is hard to envisage that such a small amount would be sufficient to account for the observed biological activity that involves a substantial fraction (>30%) of the XPA proteins actually participating in NER (Fig. 4). The absence of (significant quantities of) preassembled NER holocomplexes containing XPA (as determined here) in living cells contrasts with the results of an earlier biochemical study of *Saccharomyces cerevisiae* in which a completely assembled NER complex was identified (54). It is, however, not excluded that part of the XPA molecules are present in smaller, transient complexes, as reported previously (3, 16, 23, 61). Several explanations may account for these differences. First, during cell lysis and extract preparation, ionic-strength and local concentrations are different from those in the in vivo situation. In addition, competing factors, or natural substrates, such as DNA and/or chromatin, are absent. This will affect (and may even enhance) associations between proteins with an intrinsic affinity for each other, influencing copurification and immunoprecipitation behavior. Second, many reported interactions between NER factors are based on two-hybrid screens or immobilized factors on column matrices (reviewed in references 5 and 15). In both of these cases, high local concentrations of one NER factor will artificially shift the association-dissocia-tion equilibrium to the side of binding. Finally, the process of an ordered repair complex assembly in mammalian nuclei (60) might differ from the situation in yeast cells due to differences in genome size and nuclear structure.

Transient immobilization of GFP-XPA in DNA repair

Here we provide evidence that GFP-XPA immobilization is linked to actual repair and involves sequential NER complex assembly on DNA lesions in living cells. Immobilization of GFP-XPA is likely due to either direct sequestration to damaged DNA or entrapment into NER reaction intermediates. First, free diffusing GFP-XPA became partially immobilized when DNA damage was inflicted by UV light. Our in vivo results are consistent with the previously reported binding of XPA to nuclear structures after UV irradiation as determined by reduced Triton X-100 extractability on fixed cells (55). Second, the UV-induced immobilization is found specifically for NER factors and is not noted with other proteins, such as transcription activators and proteins implicated in other repair pathways (19, 29). Third, the fraction of immobilized GFP-XPA appears to depend on the number of lesions induced by UV irradiation. Fourth, we observed a time-dependent reduction of the amount of trapped GFP-XPA after UV irradiation, with no significant binding 24 h post-UV exposure. This is in agreement with the notion that when DNA repair proceeds, fewer target sites are available for binding GFP-XPA. Fifth, as discussed below, XPA immobilization does not occur in an XPC-deficient background. Finally, we visualized a fast recruitment of GFP-XPA to areas of local UV damage in nuclei of living cells. FLIP measurements indicated that GFP-XPA molecules reside for approximately 4 to 6 min within these locally damaged sites.

The transient UV dose-dependent immobilization of GFP-tagged ERCC1 in CHO cells and that of GFP-XPA analyzed here in human cells show comparable kinetics in terms of the maximum fraction of molecules that become immobilized and the UV dose at which both reach a plateau. The rate at which both proteins accumulate in damaged regions of nuclei (data not shown) and their residence time at these areas are quite similar as well. The observed comparable reaction kinetics, on rate, binding time, and substrate (UV damage) dependency suggest that both factors enter the NER complex, stay bound, and are subsequently released from the DNA lesion-NER complex at about the same time. A marked difference, however, is that in the CHO cell line expressing ERCC1-GFP the total repair time (i.e., time after UV irradiation where no notable immobilization of ERCC1-GFP is observed anymore) is significantly shorter than in the case of GFP-XPA. This difference is likely due to the virtual absence of CPD removal of nontranscribed DNA (GGR) in rodent cells, in contrast to the more complete repair of CPDs in human cells (31).

Order of NER factor assembly

Both UV-dependent immobilization (Fig. 7A and B) and accumulation of GFP-XPA at nuclei with local UV damage depend on the presence of XPC (Fig. 7C to H). These findings provide in vivo evidence supporting the results of previous biochemical studies indicating that the action of XPC/hHR23B precedes the XPA involvement in NER (6, 52, 53, 64). They are also in line with previous immunocytochemistry analysis results (60) indicating that assembly of various NER factors (XPA, TFIIH, ERCC1/XPF, and XPG) at a local damaged area is dependent on XPC.

The major, and perhaps only difference between TCR and GGR is based on the (initial) recognition step. It is therefore also likely that the factors that are different in the two pathways, i.e., XPC/hHR23B (and for some lesions UV-DDB [or XPE]) (56) and the CS factors, respectively, for GGR and TCR, are the respective damage sensors for both NER subpathways. In addition, XP group A cells are deficient in both GGR and TCR, whereas XP-C and CS cells are selectively defective in GGR and TCR, respectively, which argues against an initial damage-sensing role for XPA. Since XPC only accounts for GGR, it is surprising that in XP-C cells, no local accumulation of GFP-XPA was observed, whereas these cells have a normal functional TCR. Apparently, the contribution of TCR in these cells is too low to be detected by the currently applied immunocytochemistry procedure using local irradiation or FRAP-FIM techniques.

Surprisingly, we also found that RPA is localized to UV-damaged subnuclear regions in the absence of XPA, suggesting that at least for the loading of RPA into the NER preincision complex, association to XPA is not required. In addition to the observed diffusion rates of GFP-XPA, it is therefore conceivable that the majority of XPA and RPA are not complexed prior to binding to the NER lesion. In view of the multiple roles of RPA, it is also plausible that association of RPA to its interacting partners, here XPA, only occurs after entrance to the specific site of action.

Furthermore, local accumulation of RPA to UV-damaged areas seemed to depend on functional XPC, whereas XPA and XPG appeared to be dispensable for this relocalization. However, it cannot be excluded that the severely truncated XPG protein present in XP-G/CS cells is sufficient to (make it possible to) recruit RPA to the NER complex. A further point of interest is the observation that the functionality of the helicase subunits of TFIIH (XPB and XPD), which cause the formation of a single-stranded DNA region around the lesion that could theoretically attract RPA to the site of NER, is in fact dispensable for this recruitment. Our results therefore indicate that RPA is also not incorporated into the forming NER complex on the basis of its

affinity for this single-stranded DNA region only but may require protein-protein interactions of early NER factors. These findings raise the question as to what causes the entry of RPA into the NER complex, i.e., which protein(s) or protein function(s) is necessary and indispensable for RPA to be recruited to the NER complex, and the timing of this entry. Theoretically, given our findings, it is possible that RPA enters the NER complex as the third protein (complex), after XPC/hHR23B/centrin 2 and TFIIH, in order to be incorporated into the NER incision complex. At present, however, we cannot exclude the possibility that the XPG protein precedes this step.

Advantages of a sequential assembly model for NER

This work combined with our group's previous study (29) shows that repair factors XPA and ERCC1/XPF participate in NER by a temporary entrapment of free diffusing proteins into NER-DNA lesion complexes. These results favor an 'assembly on the spot' model for individual NER factors rather than a model of preassembled NER complexes. Preassembled 'repairosomes' might be considered to be efficient 'machines' ready to act on demand. On the other hand, dynamic assembly and disassembly of molecular complexes allows a more combinatorial flexibility of the reaction constituents that participate in other mechanisms. This is particularly relevant for NER, since almost all NER factors, except XPA, are known to participate also in other DNA-metabolizing processes. TFIIH and CSB are involved in transcription (50, 58), ERCC1/XPF functions also in recombination repair (46), XPG plays an additional role in base excision repair, BER (12, 36), and the single-stranded DNA binding protein hRPA acts in almost every DNA transaction. The latter is perhaps the prototype of a multilateral factor, since this hRPA functions in at least replication, NER, BER, and homologous recombination (34, 40). The different repair proteins (from BER, NER, and doublestrand break repair) interact with a common small domain of this protein, arguing for a competitive association with RPA, rather than divers preassembled subcomplexes including RPA specific for each cellular function. A distributive, diffusion-driven model has the advantage of permitting efficient usage and quick switching of proteins or protein complexes between distinct nuclear processes. An additional important advantage of sequential assembly of NER factors is that it allows regulation at multiple levels.

The involvement of many NER factors in other processes may imply that the basic rules learned here for NER are also applicable to those other systems, at least when shared NER factors are concerned. Nuclear processes, such as replication and transcription, are scheduled and confined or initiated at specific loci in the genome. These mechanisms may require structural nuclear elements that coordinate their specific spatial and temporal actions. High local concentrations of specific factors have indeed been found, and models have been put forward in which DNA is pulled through these 'factories' (11). However, such a spatiotemporal regulation might be less beneficial for repair than for replication and transcription, since repair has to act at any location in the genome at any moment in the cell cycle. Free diffusion of repair factors and binding when affinity is increased by a structural change (lesion) seems to be more efficient than tracking along relatively crowded DNA stretches or chromatin fibers by large complexes over long distances before they encounter injuries. However, a partial scanning mode of action is not excluded for all NER factors. Lesion detection within TCR is by definition performed by a DNA-tracking RNA polymerase II elongation complex. A similar scenario for the initial step in GGR can be envisaged.

Acknowledgements

We thank Leon Mullenders and Roel van Driel for support and stimulating discussion and K. Tanaka, Osaka, Japan and O. Nikaido, Kanazawa, Japan for kindly providing polyclonal XPA antisera and anti-CPD monoclonal antibodies, respectively.

This work was supported by grant NWO-ALW 805-33-441-P and investment grants NWO GB-MW 903-68-370 and 901-01-229 from The Netherlands Organization for Scientific Research, by The Dutch Cancer Society (KWF) EUR 1999-2004, and by the Louis Jeantet Foundation.

References

1. Aboussekhra, A., M. Biggerstaff, M.K.K. Shivji, J.A. Vilpo, V. Moncollin, V.N. Podust, M. Protic, U. Hubscher, J.M. Egly, and R.D. Wood (1995). Mammalian DNA nucleotide excision repair reconstituted with purified components. Cell *80*:859–68.
2. Araki, M., C. Masutani, M. Takemura, A. Uchida, K. Sugasawa, J. Kondoh, Y. Ohkuma, and F. Hanaoka (2001). Centrosome protein centrin 2/caltractin 1 is part of the xeroderma pigmentosum group C complex that initiates global genome nucleotide excision repair. J. Biol. Chem. *276*:18665–72.
3. Araujo, S. J., E.A. Nigg, and R.D. Wood (2001). Strong functional interactions of TFIIH with XPC and XPG in human DNA nucleotide excision repair, without a preassembled repairosome. Mol. Cell. Biol. *21*:2281–91.
4. Araujo, S.J., F. Tirode, F. Coin, H. Pospiech, J.E. Syvaoja, M. Stucki, U. Hubscher, J.M. Egly, and R.D. Wood (2000. Nucleotide excision repair of DNA with recombinant human proteins: definition of the minimal set of factors, active forms of TFIIH, and modulation by CAK. Genes Dev. *14*:349–59.
5. Araujo, S.J., and R.D. Wood (1999). Protein complexes in nucleotide excision repair. Mutat. Res. *435*:23–33.
6. Batty, D., V. Rapic'-Otrin, A.S. Levine, and R.D. Wood (2000). Stable binding of human XPC complex to irradiated DNA confers strong discrimination for damaged sites. J. Mol. Biol. *300*:275–90.
7. Bootsma, D., K.H. Kraemer, J.E. Cleaver, and J.H.J. Hoeijmakers (2001). Nucleotide excision repair syndromes: xeroderma pigmentosum, Cockayne syndrome and trichothiodystrophy, p. 677–703. In B. Vogelstein and K.W. Kinzler, ed., The genetic basis of human cancer, 8th ed. McGraw-Hill, New York, N.Y.
8. Bowman, K.K., D.M. Sicard, J.M. Ford, and P.C. Hanawalt (2000). Reduced global genomic repair of ultraviolet light-induced cyclobutane pyrimidine dimers in simian virus 40-transformed human cells. Mol. Carcinog. *29*:17–24.
9. Chu, G., and E. Chang (1988). Xeroderma pigmentosum group E cells lack a nuclear factor that binds to damaged DNA. Science *242*:564–7.
10. Citterio, E., W. Vermeulen, and J.H.J. Hoeijmakers (2000). Transcriptional healing. Cell *101*:447–50.
11. Cook, P.R. (1999). The organization of replication and transcription. Science *284*:1790–5.
12. Cooper, P.K., T. Nouspikel, S.G. Clarkson, and S.A. Leadon (1997). Defective transcription-coupled repair of oxidative base damage in Cockayne syndrome patients from XP group G. Science *275*:990–3.
13. Boer, J. de, and J.H.J. Hoeijmakers (2000). Nucleotide excision repair and human syndromes. Carcinogenesis *21*:453–60.
14. Laat, W.L. de, E. Appeldoorn, K. Sugasawa, E. Weterings, N.G. Jaspers, and J.H.J. Hoeijmakers (1998). DNA-binding polarity of human replication protein A positions nucleases in nucleotide excision repair. Genes Dev. *12*:2598–609.
15. Laat, W.L. de, N.G. Jaspers, and J.H. Hoeijmakers (1999). Molecular mechanism of nucleotide excision repair. Genes Dev. *13*:768–85.

16. Drapkin, R., J.T. Reardon, A. Ansari, J.C. Huang, L. Zawel, K. Ahn, A. Sancar, and D. Reinberg (1994). Dual role of TFIIH in DNA excision repair and in transcription by RNA polymerase II. Nature *368*:769–72.
17. Eker, A.P.M., W. Vermeulen, N. Miura, K. Tanaka, N.G.J. Jaspers, J.H.J. Hoeijmakers, and D. Bootsma (1992). Xeroderma pigmentosum group A correcting protein from calf thymus. Mutat. Res. *274*:211–24.
18. Ellenberg, J., E.D. Siggia, J.E. Moreira, C.L. Smith, J.F. Presley, H.J. Worman, and J. Lippincott-Schwartz (1997). Nuclear membrane dynamics and reassembly in living cells: targeting of an inner nuclear membrane protein in interphase and mitosis. J. Cell Biol. *138*:1193–206.
19. Essers, J., A.B. Houtsmuller, L. van Veelen, C. Paulusma, A.L. Nigg, A. Pastink, W. Vermeulen, J.H.J. Hoeijmakers, and R. Kanaar (2002). Nuclear dynamics of RAD52 group homologous recombination proteins in response to DNA damage. EMBO J. *21*:2030–7.
20. Evans, E., J.G. Moggs, J.R. Hwang, J.M. Egly, and R.D. Wood (1997). Mechanism of open complex and dual incision formation by human nucleotide excision repair factors. EMBO J. *16*:6559–73.
21. Friedberg, E.C., G.C. Walker, and W. Siede (1995). DNA repair and mutagenesis. ASM Press, Washington, D.C.
22. Frit, P., E. Bergmann, and J.M. Egly (1999). Transcription factor IIH: a key player in the cellular response to DNA damage. Biochimie *81*:27–38.
23. Gool, A.J. van, G. T. J. Van der Horst, E. Citterio, and J. H. J. Hoeijmakers,1997). Cockayne syndrome: defective repair of transcription? EMBO J. 16: 4155–4162.
24. Guzder, S.N., P. Sung, L. Prakash, and S. Prakash (1996). Nucleotide excision repair in yeast is mediated by sequential assembly of repair factors and not by a pre-assembled repairosome. J. Biol. Chem. *271*:8903–10.
25. Hamel, B.C., A. Raams, A.R. Schuitema-Dijkstra, P. Simons, I. van der Burgt, N.G. Jaspers, and W.J. Kleijer (1996). Xeroderma pigmentosum-Cockayne syndrome complex: a further case. J. Med. Genet. *33*:607–10.
26. Hanawalt, P., and G. Spivak (1999). Transcription-coupled DNA repair. In M. Dizdaroglu and A.E. Karakaya, ed., Advances in DNA damage and repair. Kluwer Academic/Plenum Publishers, New York, N.Y.
27. He, Z., L.A. Henricksen, M.S. Wold, and C.J. Ingles (1995). RPA involvement in the damage-recognition and incision steps of nucleotide excision repair. Nature *374*:566–9.
28. Hoeijmakers, J.H.J. (2001). Genome maintenance mechanisms for preventing cancer. Nature *411*:366–74.
29. Hoogstraten, D., A.L. Nigg, H. Heath, L.H. Mullenders, R. van Driel, J.H.J. Hoeijmakers, W. Vermeulen, and A.B. Houtsmuller (2002). Rapid switching of TFIIH between RNA polymerase I and II transcription and DNA repair in vivo. Mol. Cell *10*:1163–74.
30. Houtsmuller, A.B., S. Rademakers, A.L. Nigg, D. Hoogstraten, J.H.J. Hoeijmakers, and W. Vermeulen (1999). Action of DNA repair endonuclease ERCC1/XPF in living cells. Science *284*:958–61.
31. Houtsmuller, A.B., and W. Vermeulen (2001). Macromolecular dynamics in living cell nuclei revealed by fluorescence redistribution after photobleaching. Histochem. Cell Biol. *115*:13–21.
32. Hwang, B.J., J.M. Ford, P.C. Hanawalt, and G. Chu (1999). Expression of the p48 xeroderma pigmentosum gene is p53-dependent and is involved in global genomic repair. Proc. Natl. Acad. Sci. USA *96*:424–8.
33. Iyer, N., M.S. Reagan, K.-J. Wu, B. Canagarajah, and E.C. Friedberg (1996). Interactions involving the human RNA polymerase II transcription/nucleo-tide excision repair complex TFIIH, the nucleotide excision repair protein XPG, and Cockayne syndrome group B, CSB protein. Biochemistry *35*: 2157–67.
34. Keeney, S., G.J. Chang, and S. Linn (1993). Characterization of human DNA damage binding protein implicated in xeroderma pigmentosum E. J. Biol. Chem. *268*:21293–300.
35. Kowalczykowski, S.C. (2000). Some assembly required. Nat. Struct. Biol. *7*:1087–9.
36. Kusumoto, R., C. Masutani, K. Sugasawa, S. Iwai, M. Araki, A. Uchida, T. Mizukoshi, and F. Hanaoka (2001). Diversity of the damage recognition step in the global genomic nucleotide excision repair in vitro. Mutat. Res. *485*: 219–27.

37. Le Page, F., E.E. Kwoh, A. Avrutskaya, A. Gentil, S.A. Leadon, A. Sarasin, and P.K. Cooper (2000). Transcription-coupled repair of 8-oxoguanine: requirement for XPG, TFIIH, and CSB and implications for Cockayne syndrome. Cell *101*:159–71.
38. Li, L., X. Lu, C.A. Peterson, and R.J. Legerski (1995). An interaction between the DNA repair factor XPA and replication protein A appears essential for nucleotide excision repair. Mol. Cell. Biol. *15*:5396–402.
39. Lindahl, T., and R.D. Wood (1999). Quality control by DNA repair. Science *286*:1897–905.
40. Matsuda, T., M. Saijo, I. Kuraoka, T. Kobayashi, Y. Nahatssu, A. Nagai, T. Enjoji, C. Masutani, K. Sugasawa, F. Hanaoka, A. Yasui, and K. Tanaka (1995). DNA repair protein XPA binds to replication protein A, RPA. J. Biol. Chem. *270*:4152–7.
41. Mer, G., A. Bochkarev, R. Gupta, E. Bochkareva, L. Frappier, C. J. Ingles, A.M. Edwards, and W.J. Chazin (2000). Structural basis for the recognition of DNA repair proteins UNG2, XPA, and RAD52 by replication factor RPA. Cell *103*:449–56.
42. Missura, M., T. Buterin, R. Hindges, U. Hubscher, J. Kasparkova, V. Brabec, and H. Naegeli (2001). Double-check probing of DNA bending and unwinding by XPA-RPA: an architectural function in DNA repair. EMBO J. *20*:3554–64.
43. Miura, N., I. Miyamoto, H. Asahina, I. Satokata, K. Tanaka, and Y. Okada (1991). Identification and characterization of XPAC protein, the gene product of the human XPAC, xeroderma pigmentosum group A complementing gene. J. Biol. Chem. *266*:19786–9.
44. Mone, M. J., M. Volker, O. Nikaido, L.H. Mullenders, A. A. van Zeeland, P.J. Verschure, E.M. Manders, and R. van Driel (2001). Local UV-induced DNA damage in cell nuclei results in local transcription inhibition. EMBO Rep. *2*:1013–7.
45. Mu, D., C.H. Park, T. Matsunaga, D.S. Hsu, J.T. Reardon, and A. Sancar (1995). Reconstitution of human DNA repair excision nuclease in a highly defined system. J. Biol. Chem. *270*:2415–8.
46. Nakatsu, Y., H. Asahina, E. Citterio, S. Rademakers, W. Vermeulen, S. Kamiuchi, J.P. Yeo, M.C. Khaw, M. Saijo, N. Kodo, T. Matsuda, J.H.J. Hoeijmakers, and K. Tanaka (2000). XAB2, a novel tetratricopeptide repeat protein involved in transcription-coupled DNA repair and transcription. J. Biol. Chem. *275*:34931–7.
47. Niedernhofer, L.J., J. Essers, G. Weeda, B. Beverloo, J. de Wit, M. Muijtjens, H. Odijk, J.H.J. Hoeijmakers, and R. Kanaar (2001). The structurespecific endonuclease Ercc1-Xpf is required for targeted gene replacement in embryonic stem cells. EMBO J. *20*:6540–9.
48. Patrick, S.M., and J.J. Turchi (2002). Xeroderma pigmentosum complementation group A protein, XPA modulates RPA-DNA interactions via enhanced complex stability and inhibition of strand separation activity. J. Biol. Chem. *277*:16096–101.
49. Reardon, J. T., and A. Sancar (2002). Molecular anatomy of the human excision nuclease assembled at sites of DNA damage. Mol. Cell. Biol. *22*:5938–45.
50. Robins, P., C.J. Jones, M. Biggerstaff, T. Lindahl, and R.D. Wood (1991). Complementation of DNA repair in xeroderma pigmentosum group A cell extracts by a protein with affinity for damaged DNA. EMBO J. *10*:3913–21.
51. Schaeffer, L., R. Roy, S. Humbert, V. Moncollin, W. Vermeulen, J.H.J. Hoeijmakers, P. Chambon, and J.M. Egly (1993). DNA repair helicase: a component of BTF2, TFIIH basic transcription factor. Science *260*:58–63.
52. Selby, C.P., and A. Sancar (1997). Human transcription-repair coupling factor CSB/ERCC6 is a DNA-stimulated ATPase but is not a helicase and does not disrupt the ternary transcription complex of stalled RNA polymerase II. J. Biol. Chem. *272*:1885–90.
53. Spek, P. J. van der, A. Eker, S. Rademakers, C. Visser, K. Sugasawa, C. Masutani, F. Hanaoka, D. Bootsma, and J.H.J. Hoeijmakers (1996). XPC and human homologs of RAD23: intracellular localization and relationship to other nucleotide excision repair complexes. Nucleic Acids Res. *24*:2551–9.
54. Sugasawa, K., J.M. Ng, C. Masutani, S. Iwai, P.J. van der Spek, A.P. Eker, F. Hanaoka, D. Bootsma, and J.H.J. Hoeijmakers (1998). Xeroderma pigmentosum group C protein complex is the initiator of global genome nucleotide excision repair. Mol. Cell *2*:223–32.

55. Sugasawa, K., T. Okamoto, Y. Shimizu, C. Masutani, S. Iwai, and F. Hanaoka (2001). A multistep damage recognition mechanism for global genomic nucleotide excision repair. Genes Dev. *15*:507–21.
56. Svejstrup, J.Q., Z.G. Wang, W.J. Feaver, X.H. Wu, D.A. Bushnell, T.F. Donahue, E.C. Friedberg, and R.D. Kornberg (1995). Different forms of TFIIH for transcription and DNA repair: holo-TFIIH and a nucleotide excision repairosome. Cell *80*:21–8.
57. Svetlova, M., A. Nikiforov, L. Solovjeva, N. Pleskach, N. Tomilin, and P.C. Hanawalt (1999). Reduced extractability of the XPA DNA repair protein in ultraviolet light-irradiated mammalian cells. FEBS Lett. *463*:49–52.
58. Tang, J. Y., B.J. Hwang, J.M. Ford, P.C. Hanawalt, and G. Chu (2000). Xeroderma pigmentosum p48 gene enhances global genomic repair and suppresses UV-induced mutagenesis. Mol. Cell *5*:737–44.
59. Vermeulen, W., A.J. van Vuuren, M. Chipoulet, L. Schaeffer, E. Appeldoorn, G. Weeda, N.G. Jaspers, A. Priestley, C.F. Arlett, A.R. Lehmann, M. Stefeanini, M. Mezzina, A. Sarasin, D. Bootsma, J.M. Egly, and J.H.J. Hoeijmakers (1994). Three unusual repair deficiencies associated with transcription factor BTF2(TFIIH: evidence for the existence of a transcription syndrome. Cold Spring Harbor Symp. Quant. Biol. *59*:317–29.
60. Volker, M., M.J. Moné, P. Karmakar, A. Hoffen, W. Schul, W. Vermeulen, J.H.J. Hoeijmakers, R. van Driel, A.A. van Zeeland, and L.H.F. Mullenders (2001). Sequential assembly of the nucleotide excision repair factors in vivo. Mol. Cell *8*:213–24.
61. Wakasugi, M., and A. Sancar (1999). Order of assembly of human DNA repair excision nuclease. J. Biol. Chem. *274*:18759–68.
62. Wakasugi, M., M. Shimizu, H. Morioka, S. Linn, O. Nikaido, and T. Matsunaga (2001). Damaged DNA-binding protein DDB stimulates the excision of cyclobutane pyrimidine dimers in vitro in concert with XPA and replication protein A. J. Biol. Chem. *276*:15434–40.
63. Wansink, D.G., W. Schul, I. van der Kraan, B. van Steensel, R. van Driel, and L. de Jong (1993). Fluorescent labeling of nascent RNA reveals transcription by RNA polymerase II in domains scattered throughout the nucleus. J. Cell Biol. *122*:283–93.
64. Yokoi, M., C. Masutani, T. Maekawa, K. Sugasawa, Y. Ohkuma, and F. Hanaoka (2000). The xeroderma pigmentosum group C protein complex XPC-HR23B plays an important role in the recruitment of transcription factor IIH to damaged DNA. J. Biol. Chem. *275*:9870–5.